Biomaterials 37 (2015) 415–424

Contents lists available at ScienceDirect

Biomaterials

journal homepage: www.elsevier.com/locate/biomaterials

Dynamic imaging of PEGylated indocyanine green (ICG) liposomes within the tumor microenvironment using multi-spectral optoacoustic tomography (MSOT)

Nicolas Beziere [a, 1], Neus Lozano [b, c, 1], Antonio Nunes [a], Juan Salichs [a], Daniel Queiros [a], Kostas Kostarelos [b, c, **], Vasilis Ntziachristos [a, *]

[a] Institute for Biological and Medical Imaging (IBMI), Technische Universität München and Helmholtz Zentrum München, Ingolstädter Landstrasse 1, 85764 Neuherberg, Germany
[b] Nanomedicine Lab, Faculty of Medical & Human Sciences, University of Manchester, AV Hill Building, Manchester M13 9PT, UK
[c] UCL School of Pharmacy, Faculty of Life Sciences, University College London, Brunswick Square, London WC1N 1AX, UK

ARTICLE INFO

Article history:
Received 21 July 2014
Accepted 2 October 2014
Available online 23 October 2014

Keywords:
Tumor
Optoacoustic
Photoacoustic
Liposome
Indocyanine green
Imaging

ABSTRACT

Multispectral optoacoustic tomography (MSOT) is a powerful modality that allows high-resolution imaging of photo-absorbers deep within tissue, beyond the classical depth and resolution limitations of conventional optical imaging. Imaging of intrinsic tissue contrast can be complemented by extrinsically administered gold nanoparticles or fluorescent molecular probes. Instead, we investigated herein generation of re-engineered clinically-used PEGylated liposomes incorporating indocyanine green (LipoICG) as a contrast strategy that combines materials already approved for clinical use, with strong photo-absorbing signal generation available today only from some metallic nanoparticles (e.g. gold nanorods). Using MSOT we confirmed LipoICG as a highly potent optoacoustic agent and resolved tissue accumulation in tumor-bearing animals over time with high-sensitivity and resolution using two tumor models of different vascularisation. We further showcase a paradigm shift in pharmacology studies and nanoparticle investigation, by enabling detailed volumetric optical imaging *in vivo* through the entire tumor tissue non-invasively, elucidating never before seen spatiotemporal features of optical agent distribution. These results point to LipoICG as a particle with significant advantageous characteristics over gold nanoparticles and organic dyes.

1. Introduction

Since the original description of phospholipid self-assembly into closed bilayer vesicles in aqueous media [1], liposomes have received significant attention as drug delivery systems and made considerable contributions in various fields including clinical medicine [2]. Their versatility to cargo either hydrophilic (entrapped in the inner aqueous core) or hydrophobic (incorporated within the lipid bilayer) entities, combined with tunable size and surface properties have proven clinically useful [2–4]. Liposomes have been engineered to circulate longer in the bloodstream and evade capture by the reticulo-endothelial system, typically using polyethylene glycol (PEG) grafting on their outer surface [5]. These surface-modified nanoscale vesicles have been applied to transport of anti-neoplastic small molecules, such as doxorubicin (Doxil®), clinically used against various cancer indications [6,7]. PEGylated nanoparticles, including liposomes, have been described to preferentially accumulate within the interstitium of tissues with a leaky vascular bed (e.g. some tumors, infarcted or inflamed sites, disrupted blood–brain barrier) via the enhanced permeation and retention (EPR) effect [8].

Despite the widespread utilization of liposomes, there have been challenges in assessing their interstitial tissue localization and distribution *in vivo* [9–11]. Liposome visualization *in vivo* relies on their labeling with contrast agents. Paramagnetic agents, such as gadolinium [12] or manganese [13], have been employed for high-resolution MRI-based particle mapping, however such approaches suffer from low sensitivity, and generally require doses in the order of 100 μg/kg of metal. Iodine-based liposome loading has been investigated for CT imaging, but excessive concentrations were also

* Corresponding author. Tel.: +49 89 3187 3852.
** Corresponding author. Tel.: +44 161 275 1800.
E-mail addresses: kostas.kostarelos@manchester.ac.uk (K. Kostarelos), v.ntziachristos@tum.de (V. Ntziachristos).
[1] These authors contributed equally to this work.

http://dx.doi.org/10.1016/j.biomaterials.2014.10.014
0142-9612/

reported [14,15]. Typically, the labeled liposome distribution is obtained as a difference image, i.e. a subtraction of an image obtained before liposome administration (baseline image) from an image obtained after liposome administration. The need for baseline measurements makes long-term longitudinal studies impractical and sensitive to motion with time. The use of radiotracers for PET and SPECT imaging has been considered as a higher sensitivity alternative to MRI and CT [11,16]. Nuclear imaging however, suffers from low spatial resolution and the relatively short time-course allowed for imaging due to the energy-decaying radionuclides employed, in particular with ^{18}F nuclear tracers, although alternatives such as ^{89}Zc are explored as longer half-life alternatives. Gamma-ray imaging has provided valuable data on tissue distribution and the pharmacokinetic profile of radiolabelled liposomes, however was limited in revealing interstitial localization within tissues and accumulation over several days. Epi-illumination fluorescence imaging [17,18] of fluorescently-labeled liposomes has also been considered, but is limited to qualitative observations of surface recorded activity. Overall, current imaging modalities exhibit limitations in studying nanoparticle distribution in high-resolution and over time, as has been recently pointed out by others [9].

Using recent advances in instrumentation, image reconstruction and spectral unmixing techniques, Multispectral Optoacoustic Tomography (MSOT) is emerging as a potent modality for visualization in nanomedicine [19]. Using spectral differentiation, MSOT can enable sensing of optical contrast at the absence of baseline measurements, at high resolution. This is a unique combination of imaging features, not available to other imaging methods, and is ideally suited for sensing optical contrast in three dimensions. Intrinsic MSOT tissue contrast is attributed primarily to hemoglobin, melanin, water and lipids. Contrast enhancement can be achieved by metal nanoparticles (most notably gold), organic chromophores and fluorochromes, as well as non-metallic nanoparticles [20–22]. Fluorochromes, while preferred for labeling in preclinical and clinical optical imaging, are not strong optoacoustic signal generators. Due to plasmon resonance, gold nanoparticles exhibit strong optoacoustic responses; however their path to clinical acceptance may be more problematic – due to the typically long retention times in tissues. They remain nevertheless the current standard for signal generation in optoacoustic imaging, thanks to their signal strength and photo-stability.

Liposome systems have been labeled with ICG previously [18,23,24] however solely as a fluorescent probe and only for subcutaneous or intradermal administration, intended mainly for lymph-node imaging. Moreover, there is very limited information on the methodology of ICG incorporation into liposomal bilayers. No previous study has attempted to re-engineer the clinically-used PEGylated liposomes intended for systemic blood circulation, targeting and visualization of tumors. The first goal of the present study was to investigate whether a non-metal nanoparticle composed of organic fluorescent dyes of clinical relevance could yield stronger optoacoustic signals than the “gold-standard”, i.e. gold nanoparticles. For this reason we re-engineered clinically-used PEGylated liposomes (the basis of the intra-venous drug DOXIL®), and combined them with the FDA approved fluorochrome indocyanine green (ICG). Non-covalent, molecular self-assembly principles were applied to maximize the clinical translation potential of the liposomal ICG (LipoICG) constructs. LipoICG were built as biocompatible and biodegradable vesicles, consisting of molecular components with clinically established toxicity profiles compared to other photo-absorbing nanoparticles, such as gold or carbon-based nanoconstructs. We particularly interrogated whether LipoICG could be engineered to generate strong optoacoustic signals and how such particles could measure against the most potent optoacoustic contrast agents, i.e. gold nanorods.

The second goal was to elucidate the distribution of LipoICG in tissues and the tumor environment by using MSOT. MSOT is shown herein as a modality to non-invasively study and longitudinally follow the fate of liposomes within tumors and tissues.

2. Materials and methods

2.1. Engineering of liposomal indocyanine green (LipoICG) & characterization

Liposomal ICG formulations were prepared using the lipid film hydration method followed by freeze-thawing (Fig. 1A). L-α-phosphatidylcholine, hydrogenated (HSPC, Lipoid, Germany), cholesterol (Chol, Avanti Polar Lipids, USA) and 1,2-distearoyl-sn-glycero-3-phosphoethanolamine-N-[methoxy(polyethylene glycol)-2000] (DSPE-PEG$_{2000}$, Lipoid, Germany) were dissolved in chloroform/methanol (4:1, v/v) and the organic solvents were evaporated using a rotary evaporator. The resulting thin lipid film was hydrated in 5% dextrose solution containing indocyanine green (ICG, Pulsion Medical Systems, Germany). The dispersion was freeze-thawed in six cycles and then extruded. The free ICG was removed by using a spin desalting column. The ICG incorporation efficiency (%) was determined by UV-Vis spectroscopy in a Varian Cary WinUV 50 Bio spectrophotometer (USA) after sample dilution in DMSO. Three different concentrations of ICG were incorporated into 5 mM liposomes: 25 μM (LipoICG$_{25}$), 50 μM (LipoICG$_{50}$) and 75 μM (LipoICG$_{75}$). Transmission electron microscopy (TEM) micrograph was performed with a Tecnai 12 instrument operated at 120 kV accelerating voltage. Particle diameter was measured at 25 ± 0.1 °C by a Nano ZS series HT (Malvern, UK) in back scattering mode, at 173° and $\lambda = 632.8$ nm. Stability studies for the liposomal ICG formulations were followed over 5 days in a Varian Cary winUV 50 Bio spectrophotometer (USA).

2.2. Near-infra red (IVIS) in vivo imaging

8-week old female CD-1 albino mice (ICR(CD-1), Harlan, UK) were injected intravenously via tail vein with 200 μL of free ICG and LipoICG at 25 μM (5 nmol), 50 μM (10 nmol) and 75 μM (15 nmol) ICG. Whole-body NIR fluorescence imaging was performed on clipped animals under anesthesia (2% isoflurane). Imaging was performed at 5 min, 1 h, 5 h and 24 h post-injection using an IVIS Lumina and the Living Image software (Xenogen, Caliper Life Sciences). Imaging parameters: $\lambda_{bkg} = 605$ nm, $\lambda_{exc} = 745$ nm, $\lambda_{em} = 810–875$ nm, exposure time 2 s and f/stop 2. 24 h post-injection, animals were killed by carbon dioxide overdose and liver, spleen, kidney, heart and lung were harvested and imaged at the same settings described above.

2.3. Optoacoustic phantom preparation

Cylindrical phantoms of 2 cm diameter were prepared using a gel made from distilled water containing Agar (Sigma–Aldrich, St. Louis, MO, USA) for jellification (1.3% w/w) and an intralipid 20% emulsion (Sigma–Aldrich, St. Louis, MO, USA) for light diffusion (6% v/v), resulting in a gel presenting a reduced scattering coefficient of $\mu_s' \approx 10$ cm^{-1}. A cylindrical inclusion containing the sample of approximately 3 mm diameter was put approximately in the middle of the phantom, along with a tube containing classical black ink with an optical density of around 0.2 at 800 nm for intensity measurement references.

2.4. Animal models for optoacoustic imaging experiments

All procedures involving animal experiments were approved by the Government of Upper Bavaria (ref. 55.2.1.54-2632-102-11). LipoICG$_{75}$ and ICG$_{75}$ biodistribution assay by optoacoustic imaging were performed using female CD-1 albino mice. Two xenograph tumor models were employed one representative of a slow growing tumor, using HT-29 human adenocarcinoma cells and one representing rapid growth based on 4T1 murine breast cancer cells. 8 weeks old adult female Athymic Nude-Foxn1 nude mice (Harlan, Germany) were inoculated subcutaneously in the middle of the back in the region of the upper pelvis with cell suspensions (either 0.8 million 4T1 (CRL-2539) cells or 1.5 million HT29 (ATCC-HTB-38) cells) in 50 μL PBS. Animals were imaged only after tumors reached a size of approximately 8 mm diameter.

2.5. Macroscopic multi-spectral optoacoustic tomography

All optoacoustic measurements were performed in a real-time whole-body mouse imaging MSOT system. An earlier version of the system was described previously [25]. Briefly, optical excitation was provided by a Q-switched Nd: YAG laser with a pulse duration of around 10 ns and a repetition rate of 10 Hz and a tunable range of 680–900 nm. Light was homogeneously delivered to the sample using a fiber bundle split into 10 output arms. The emitted ultrasound signal was detected using a 64 element transducer array cylindrically focused and having a central frequency of 5 MHz, allowing acquisition of transverse plane images. The fiber bundle and transducer array were stationary, and the sample could be moved to acquire different imaging planes using a moving stage. Measurements took place in a temperature controlled water bath at 34 °C for acoustic coupling, and the samples were kept dry using a thin clear polyethylene membrane attached to the sample holder. We note that more recent versions of this system utilize 256 element arrays

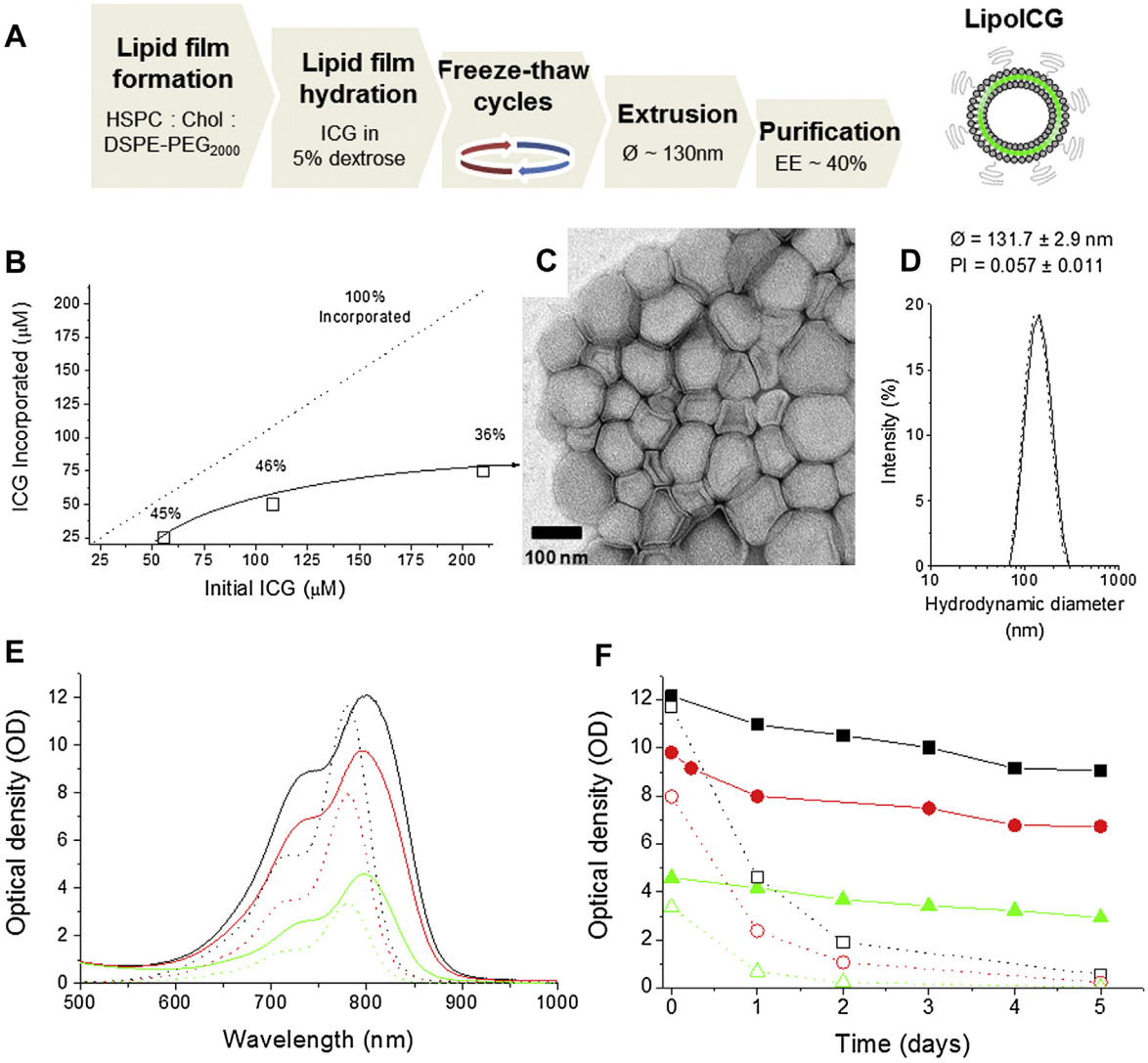

Fig. 1. Liposomal indocyanine green (LipoICG) engineering and characterization. (A) Schematic depiction of the protocol used for the incorporation of ICG in liposomes (LipoICG). The lipid film formed by HSPC:Chol:DSPE-PEG_{2000} was hydrated in 5% dextrose solution containing ICG. The dispersion was freeze-thawed and then extruded. The free ICG was removed by using a spin desalting column. (B) Concentration of ICG incorporated in the liposomes as a function of the initial ICG concentration used for the preparation of LipoICG (incorporation efficiency) for the three systems studied: $LipoICG_{75}$ (36%), $LipoICG_{50}$ (46%) and $LipoICG_{25}$ (45%). (C) TEM micrograph and (D) hydrodynamic diameter for the $LipoICG_{75}$. (E) UV-Vis absorption spectra on day of preparation and (F) maximum absorbance over 5 days of LipoICG (solid lines) and free ICG (dotted lines) at 75 μM (black lines), 50 μM (red lines) and 25 μM (green lines) ICG. (For interpretation of the references to color in this figure legend, the reader is referred to the web version of this article.)

and up to 270° mouse coverage, however this system was not available during the original phase of the studies herein.

Imaging of the phantoms was done at a single position, located approximately in the middle of the phantom. Data acquisition was performed in the wavelength range 680–900 nm in steps of 5 nm, using 10 averages per wavelength resulting in 1 s acquisition time per wavelength. Image reconstruction was based on a model based image reconstruction published previously [26,27], which delivers accurate performance and quantification over conventional back-projection algorithms. Following image reconstruction, spectral unmixing was performed using a linear model assuming that the spectra acquired were a linear mix of the ICG spectrum with background spectra. For each pixel in the image, the algorithm fitted the measured optoacoustic [28] spectrum, normalized for variations in laser energy per wavelength, to the known absorption spectra of the chromophores assumed in the image.

Animal imaging was performed under anesthesia using 1.8% isoflurane in oxygen. Data were acquired along the animal, typically acquiring cross-sectional images at one position in the liver region, one position in the kidney region, and throughout the tumor when applicable using 1 mm steps. For animal imaging, 20 averages were acquired per wavelength at 680, 710, 740, 770, 800, 830, 860 and 900 nm. Images were acquired before $LipoICG_{75}$ injection and after intravascular tail vein injection of 200 μL of $LipoICG_{75}$ corresponding to an amount of ~ 15 nmol of ICG. Post-injection images were acquired at different time points at 5 min, 1 h, 4 h and 24 h. We note that measurements acquired before $LipoICG_{75}$ injection were not used as baseline measurements but as control measurements, to examine possible cross-talk of the spectral unmixing method employed to indicate presence of $LipoICG_{75}$ Data before $LipoICG_{75}$ administration.

Semi-quantitative processing of the data was performed defining various regions of interest within a 2D image, plotting the maximum signal against time. Three regions of interest were defined: “body”, defined as the entire transverse section of the animal minus the tumor; “muscle”, defined as the muscles alongside the spine; “tumor”, defined as the core of the tumor and excluding the blood vessels on its periphery.

2.6. *Ex vivo fluorescence and histological imaging*

Following the *in vivo* imaging experiments, animals were sacrificed by Ketamine overdose and frozen to −80 °C. For validation of the *in vivo* data, *fluorescence cryosectioning imaging* (FCSI) was performed *ex vivo* on the xenografted mice after embedding them in optimal cutting temperature media (Sakura Finitek Europe B. V., Zoeterwonde, NL) to confirm the presence of LipoICG in the different organs. Similarly to the MSOT imaging geometry, FCSI sliced the frozen mice in the axial dimension, at a 500 μm micron pitch, and recorded color and fluorescence images from each slice. The FCSI system is based on a cryotome (CM 1950, Leica Microsystems, Wetzlar, Germany), fitted with a motorized spectral illumination and

multi-spectral CCD-based detection in epi-illumination mode. Fluorescence images were captured at the peak emission wavelength of indocyanine green. In the case of microscopic images validation, tumors were sliced along the coronal plane to represent better the live imaging results.

Several of the cryosection slices produced were captured on glass slides and imaged by epi-illumination fluorescence imaging using a Leica Z16 macroscopic lens. Finally, conventional hematoxylin and eosin as well as CD31 staining were also performed with a Leica DM 2500 upright microscope, and pictures taken using a Leica EC3 color camera (Leica Microsystems, Wetzlar, Germany).

3. Results

3.1. Preparation and characterization of liposomal ICG (LipoICG) contrast agents

Three LipoICG contrast agent systems based on the same type of PEGylated liposomes used in DOXIL preparations were prepared by the film hydration method followed by freeze-thawing cycles shown schematically in Fig. 1A. The same lipid composition HSPC:Chol:DSPE-PEG_{2000} (total lipid concentration of 5 mM) and increasing ICG concentrations 25 μM ($LipoICG_{25}$), 50 μM ($LipoICG_{50}$) and 75 μM ($LipoICG_{75}$) were allowed to self-assemble to form liposomes. ICG incorporation efficiencies between 36 and 46% of the added amount were achieved (Fig. 1B). Transmission electron microscopy of the $LipoICG_{75}$ (Fig. 1C) verified the formation of homogeneous unilamellar liposomes of a mean diameter consistent with that obtained with dynamic light scattering between 120–130 nm (Fig. 1D).

The absorption spectra of the three LipoICG systems were compared to free ICG of the same concentration (Fig. 1E). ICG incorporation into liposome bilayers induced a red spectral shift of 20 nm (from 780 nm to 800 nm) in 5% dextrose, attributed to the hydrophobic character of the environment (lipid bilayer core) that the ICG molecules resided in. More importantly, all three LipoICG samples were found more photo-absorbing than the equivalent free ICG in 5% dextrose. A stability study over 5 days (Fig. 1F) indicated that the free ICG peak absorbance (dotted lines) decreased sharply within the first day, while the signal intensity for the LipoICG systems remained almost constant throughout. Both the free ICG and LipoICG were also found optically stable in 50% serum, indicating structural integrity without leakage of ICG from liposomes for 3 days (at both 25 °C and 37 °C) (Figure S2). Overall, this data confirmed the significant improvement in optical signal stability offered by the LipoICG contrast agents in physiologically-relevant solutions, independent of the incorporated amount of ICG into liposomes.

3.2. LipoICG tissue distribution by NIR fluorescence (IVIS) and optoacoustic (MSOT) imaging

The LipoICG distribution profile in tissue was investigated for all three contrast agents following intra-venous (tail vein) administration in CD-1 albino female mice, compared to free ICG (Fig. 2A) using whole-body NIR fluorescence imaging with an IVIS system. Strong fluorescent signals were obtained from the body of all injected animals 5 min after administration, however, no specific tissue could be confidently identified using the IVIS imaging system. The emitted fluorescent signal for all animals decreased within 5 h and was almost completely lost after 24 h (Fig. 2A). To verify the tissue distribution of the contrast agents, all animals were euthanized at 24 h post-injection and major organs were harvested and imaged with the IVIS camera (Fig. 2B). $LipoICG_{50}$ and $LipoICG_{75}$ injections resulted in a strong fluorescent signal from the liver showing higher optical stability of liposome-ICG *in vivo*. Images of free ICG revealed complete loss of signal from all organs. To exclude the possibility of toxicity to the organs, hematoxylin and eosin stained sections were assessed for ICG_{75} and $LipoICG_{75}$ (Fig. S1). No sign of tissue necrosis, fibrosis or inflammation in any of the organs examined was found. This further indicated that ICG and LipoICG contrast agents did not lead to any acute adverse reaction.

This study also revealed herein the limitations of NIR fluorescence imaging, illustrating the superiority of MSOT over conventional optical imaging approaches. Planar NIR fluorescence imaging offers surface-weighted readings due to the increasing light attenuation in tissue as a function of depth and tissue optical property. These limitations have been previously noted [29], and led herein to a discrepancy between *in vivo* and *ex vivo* studies. In particular, whereas excised liver tissue showed strong fluorescence signals (Fig. 2B), the same liver tissue observed *in vivo* by IVIS (Fig. 2A) revealed very faint signals which were comparable with those of background noise. Indeed, Fig. 2A shows very little activity in mice after 24 h from injection with $LipoICG_{75}$, which can be misinterpreted as complete $LipoICG_{75}$ clearance. Similar results were also observed for the $LipoICG_{25}$, $LipoICG_{50}$ (Fig. 2A). This discrepancy showcases the limitation of planar epi-illumination fluorescence imaging which can lead to erroneous observations. In contrast, MSOT imaging (Fig. 2C) was able to follow agent tissue distribution over time non-invasively, more accurately detecting the liver signal and the differences between ICG_{75} and $LipoICG_{75}$, and gave a longitudinal insight on the liver metabolism of ICG and its absence in the kidneys minutes after the injection (Figure S3). This is due to its ability to accurately resolve depth at high-resolution. The MSOT findings were also consistent with the results from imaging the excised organs by IVIS (Fig. 2B). At the 24 h time point for example, clear optoacoustic signal is seen in the liver for $LipoICG_{75}$ that was only barely detected by whole-body IVIS imaging (Fig. 2A). Furthermore, MSOT revealed that LipoICG would transiently pass through the spleen, only at the early time points through the heart region, while no significant signals were detected from the kidneys (Fig. 2C). The observed tissue distribution data, even though not quantitative, were in agreement with previously published quantitative data using radiolabelled PEGylated liposomes [30,31], further indicating the validity of MSOT imaging.

3.3. LipoICG as an optoacoustic contrast agent

The light absorbing and optoacoustic properties of the most concentrated liposomal ICG formulation ($LipoICG_{75}$) were first evaluated in a tissue-mimicking phantom, using Indian ink as a reference. Fig. 3A depicts the phantom and a typical image obtained after identification of the spectral components contained in the phantom, using spectral unmixing. Fig. 3B shows the normalized absorbance spectra and optoacoustic intensity (OA) for ICG and $LipoICG_{75}$. The OA signal in the case of $LipoICG_{75}$ was broader than that for ICG alone, however the peak did not shift and the overall shape was conserved. To be able to establish the $LipoICG_{75}$ detection limit by MSOT, serial dilution of the $LipoCG_{75}$ system was performed from 6.7 to 0.3 μM ICG (Fig. 3C). The minimum $LipoICG_{75}$ concentration detectable with the MSOT was 0.6 μM, equivalent to 0.5 mg ICG/L or 3.58×10^{17} molecules ICG/L.

Comparison of the MSOT optoacoustic signal for $LipoICG_{75}$ and ICG was then undertaken using the tissue-mimicking phantom (Fig. 3D). The experimentally determined MSOT signal intensity for the $LipoICG_{75}$ was 5.4 arbitrary unit (a.u.) compared to 4.3 for the ICG alone of an equivalent concentration (see Table in Fig. 3D). That meant that for each 1 mg/L of ICG, the MSOT signal from the liposomal system was 1.3 times higher signal than from free ICG of the same concentration. Calculation of the number of ICG molecules within each $LipoICG_{75}$ vesicle and the total number of vesicles indicated that each vesicle contained 3559 ICG molecules.

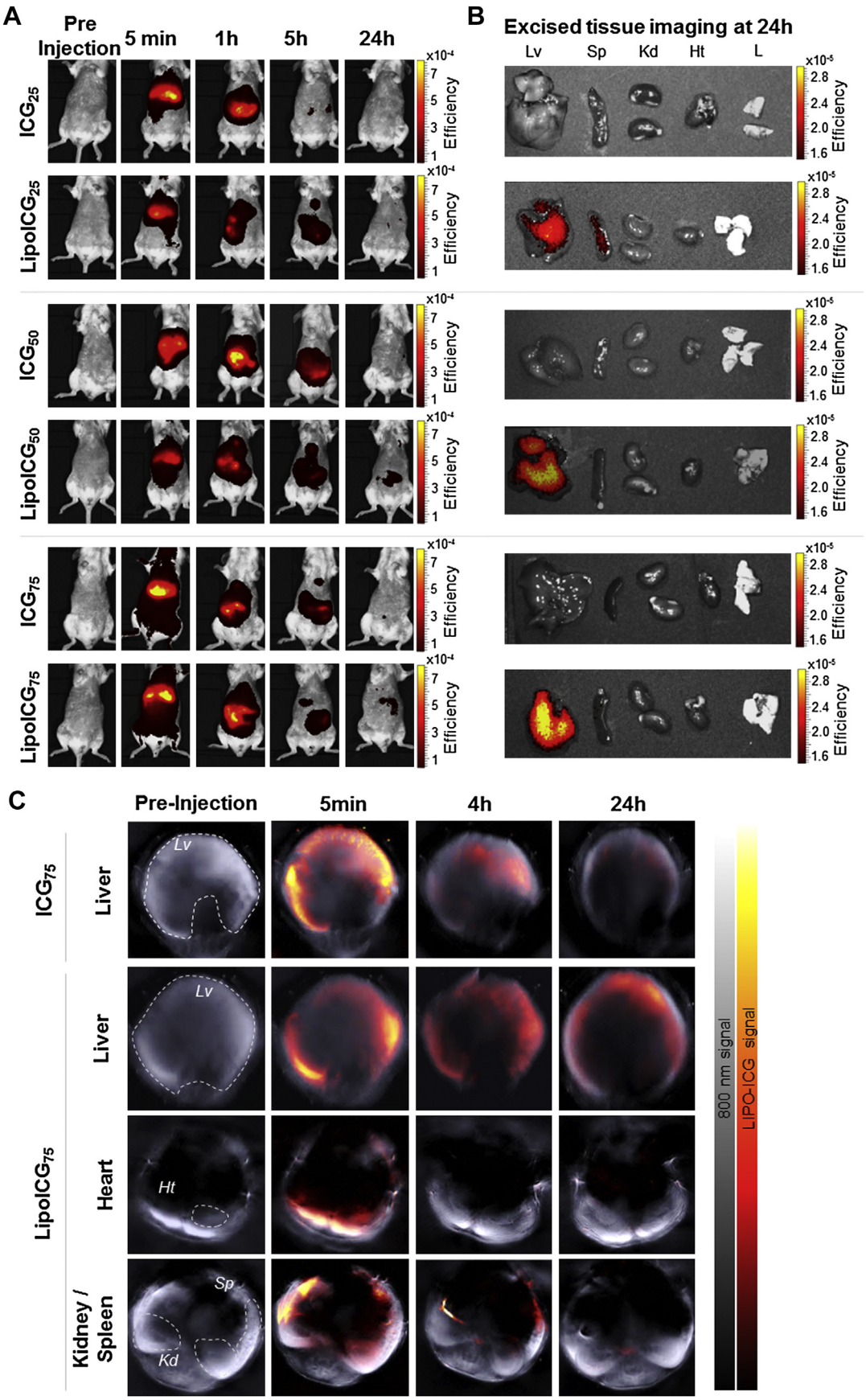

Fig. 2. Liposomal indocyanine green (LipoICG) biodistribution in a healthy animal.Whole-body near infra-red (NIR) fluorescence imaging of female CD-1 albino mice showing free ICG and LipoICG at 25, 50 and 75 μM ICG at several time points after intra-venous injection. (B) NIR fluorescence imaging of Liver (Lv), Spleen (Sp), Kidney (Kd), Heart (Ht) and Lungs (L) harvested 24 h after intra-venous injection of free ICG and LipoICG at 25, 50 and 75 μM. ICG shows high liver accumulation for LipoICG compared to ICG alone at the same ICG concentration. (C) Similar experiment performed in MSOT using ICG_{75} $LipoICG_{75}$ at the different positions. ICG_{75} and $LipoICG_{75}$ signal (hot scale) is overlayed on the anatomical image acquired at 800 nm illumination wavelength (grey scale).

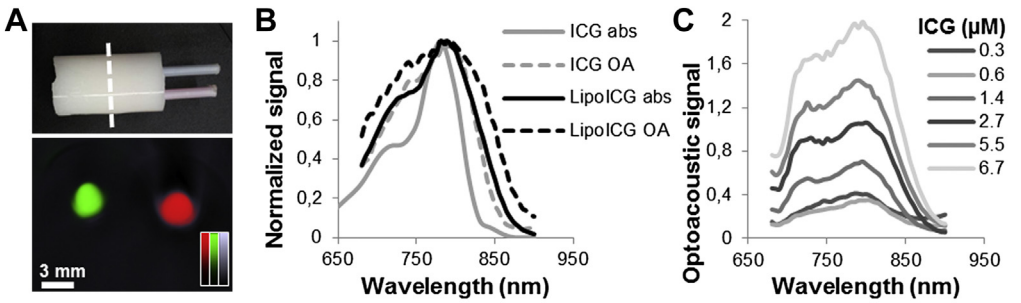

D

System	Contrast Agent Concentration (mg/L)	Number of Nanoparticles/L	Experimental OA	Calculated OA / (1mg/L)	Calculated OA / OD	Calculated OA / (1 Nanoparticle/L)
ICG	58	4.52×10^{19} molec ICG	4.3	0.074	0,36	9.51×10^{-20}
AuNRs	2450	4.70×10^{16} AuNRs	71.0	0.029	1,01	1.51×10^{-15}
LipoICG	58	1.27×10^{16} Liposomes	5.4	0.093	0,45	4.25×10^{-16}

Fig. 3. *In vitro* evaluation of liposomal indocyanine green ($LipoICG_{75}$) as an optoacoustic contrast agent. (A) Tissue mimicking phantom setup, comprising an Indian ink and a $LipoICG_{75}$ straw and the resulting optoacoustic transverse image acquired at the indicated plane, with the unmixed $LipoICG_{75}$ (green scale) and Indian ink (red scale) signal overlayed on a single wavelength image (800 nm, grey scale). (B) Normalized absorbance (abs) of ICG and $LipoICG_{75}$ compared to the normalized optoacoustic signal intensity (OA) of the same systems as acquired by MSOT. (C) MSOT optoacoustic signal obtained from serial dilution of $LipoICG_{75}$, expressed as a concentration of ICG within the liposomes. (D) Tissue phantom MSOT optoacoustic signal (OA) compared for ICG, AuNRs, and LipoICG. (For interpretation of the references to color in this figure legend, the reader is referred to the web version of this article.)

Finally gold nanorods ($AuNR_{780}$) were imaged by MSOT to benchmark the signal generation efficiency of the $LipoICG_{75}$ against the most potent and commonly used optoacoustic contrast agent today. The MSOT signal for 1 mg/L of contrast agent (ICG molecules or Au atoms in each system respectively) was higher for $LipoICG_{75}$ than for AuNRs by a factor of 3. Calculation of the signal offered by each nanoparticle (one liposome or nanorod, respectively) indicated that one AuNR was offering 3.2 times higher OA signal compared to one liposome. We then performed a similar comparative calculation of the *in vivo* conditions (injected volume, mg of contrast agent per animal; Table S1) among the three contrast agents (ICG alone, AuNR and $LipoICG_{75}$), which also take into consideration signal attenuation of the particular spectral profile of each moiety considered. The measurement indicated that in order to obtain an optimum *in vivo* MSOT signal in the case of gold nanorods [32–34] the mg of contrast agent (Au atoms) injected per animal will need to be 10 times higher compared to that (ICG molecules) for $LipoICG_{75}$, while the number of nanoparticles injected would be within the same order of magnitude (both around 2×10^{15} per animal). When looking at the optical density (Fig. 3D), LipoICG appears to provide approximately 45% of optoacoustic signal per optical density when compared to AuNR. This can be explained by looking back at the drastically different photon absorbing mechanisms regulating signal generation in organic molecules and solid metallic particles, and in that case puts LipoICG in the same order of magnitude as AuNR in terms of optoacoustic signal generation per absorbed photon.

3.4. $LipoICG_{75}$ behavior in tumor bearing animals

In a first set of experiments we macroscopically evaluated the distribution of $LipoICG_{75}$, using MSOT over time, after intra-venous administration in a 4T1 murine tumor model known for its fast growth [35]. A slower growing HT29 human colon cancer cell line [36] was similarly imaged by MSOT. The results are summarized in Fig. 4. Cross-sectional anatomical images through the mouse at the tumor area are depicted in Fig. 4A.a–j. Images acquired at 800 nm were employed for anatomic guidance and were overlayed with blood oxygenation maps (Fig. 4A.a, A.f), showing a different oxygenation pattern for the 2 tumor types. In particular the 4T1 tumor shows an intense signal of deoxygenated hemoglobin (Fig. 4A.a) and thus a hypoxic state in the core of the tumor. In contrast, milder deoxygenated hemoglobin signals are seen throughout the MSOT images of the HT29 model (Fig. 4A.f), indicative of mild perfusion throughout the tumor core. Both tumors exhibited oxygenated blood pools on their sides, indicated on Fig. 3A.a by arrows.

Fig. 4A.b–d and A.g–i show MSOT images obtained from the 4T1 and HT29 animal models after intra-venous injection of $LipoICG_{75}$. The $LipoICG_{75}$ is shown in color superimposed on anatomical cross-sectional images of the mouse obtained at 800 nm and plotted in grayscale. The presence of $LipoICG_{75}$ on the MSOT images is identified based on its absorption spectrum after spectral unmixing of MSOT images obtained at multiple wavelengths as explained in methods. $LipoICG_{75}$ provided an intense signal congruent with vascular structures identified on the anatomical image within the first minutes after injection. This is consistent with the previously reported pharmacokinetic profile of PEGylated liposomes [31] and indicated that $LipoICG_{75}$ at the early time points post-administration remained confined within the vascular system and did not localize within other tissues or deoxygenated regions of limited blood supply. At later time points, accumulation of the liposomes in the center of the 4T1 tumor can be observed (Fig. 4A.c, A.d) with a corresponding decrease of visible signal in the vasculature. The distribution of $LipoICG_{75}$ in the tumor is not homogeneous. Being a high-resolution nanoparticle imaging method, MSOT reveals that contrast enhancement using liposomes is subject to a preferential distribution and does not equally access all tumor mass. This view has more general implications in understanding treatment efficacy using nanoparticles. The heterogeneous tumor enhancement observed was consistent over time as shown in subsequent time points (Fig. 4A.d). The signal-to-noise ratio (SNR) attained by MSOT in Fig. 4A.d was 44 dB. Results appear markedly different in the HT29 tumor model, i.e. a slower

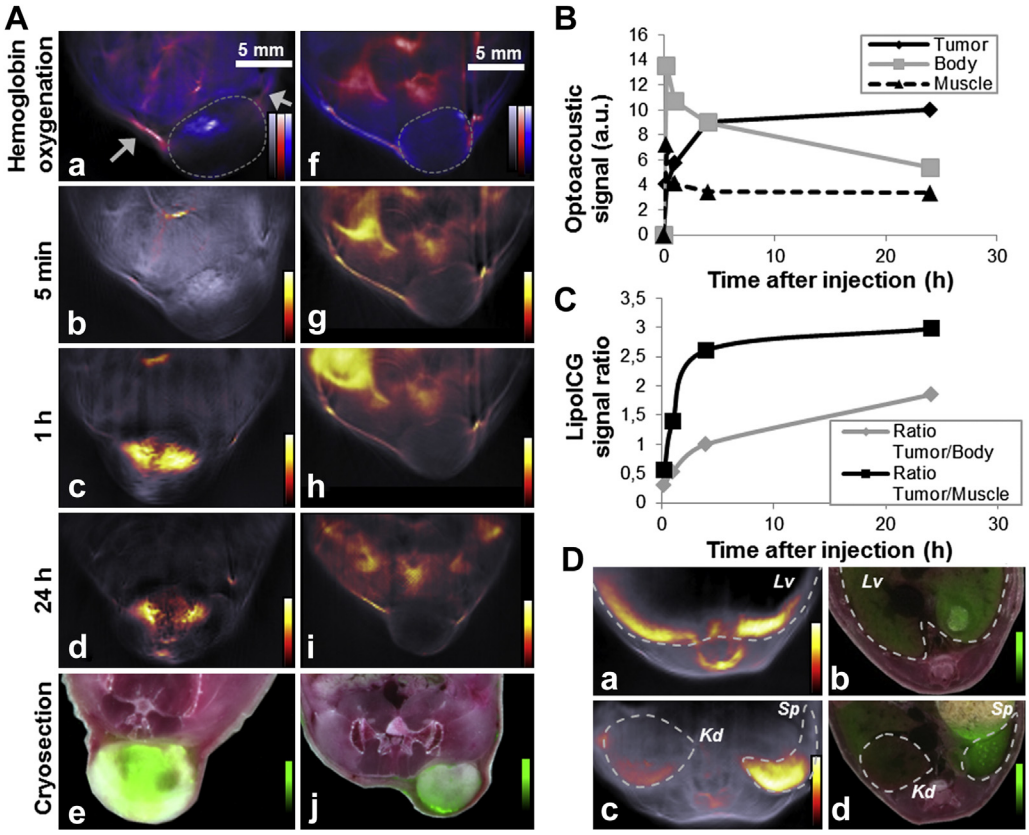

Fig. 4. Kinetics of accumulation of Liposomal ICG (LipoICG$_{75}$) in 4T1 and HT29 tumor models imaged with multi-spectral optoacoustic tomography (MSOT). (A) Transverse MSOT image of a 4T1 tumor obtained using 800 nm illumination wavelength before injection of LipoICG$_{75}$ (grey scale) overlayed with signal from hemoglobin (blue scale) and oxygenated hemoglobin (red scale) (arrows indicate the main blood vessels supplying the tumor) (a); Overlay of the MSOT LipoICG$_{75}$ signal (hot scale) on a background image (grey scale) acquired at 800 nm illumination wavelength 5 min, 1 h and 24 h after injection(b–d); Color image of a corresponding cryosection overlayed with the fluorescence signal from ICG (green scale) (e); Similar experiments performed on an HT29 tumor bearing mouse are depicted in the following column in the same arrangement(f–j). (B) Maximum LipoICG$_{75}$ signal intensity in the tumor (black line), the whole body without the tumor (grey line) and in the back muscles (dashed black line). (C) Maximum LipoICG$_{75}$ signal intensity ratio between the tumor area and the whole body (grey line) and the back muscles (black line). (D) MSOT image of the Liver (Lv) of a tumor bearing animal acquired at 800 nm acquisition wavelength and overlayed with LipoICG$_{75}$ signal (hot scale) (a); Fluorescent signal of the ICG channel (green scale) overlayed on the color picture of the cryosection in a comparable region of the liver (b); Similar layout for the images of the same animal acquired at the kidney (K.) and Spleen (Sp.) region (c–d). (For interpretation of the references to color in this figure legend, the reader is referred to the web version of this article.)

growing tumor model. As observed on Fig. 4A.g-i LipoICG$_{75}$ did not appear in the tumor core but remained peripheral to the tumor vasculature. The signal in the core of the tumor appeared so low that scaling of the images Fig. 4A.g–i instead revealed the presence of LipoICG$_{75}$, at higher amounts in other parts of the animal body, such as in the bowels, but not in the tumor core.

To validate the *in vivo* findings, the animals were euthanized after the *in vivo* MSOT imaging session at 24 h and frozen for cryosectioning. Cross-sectional cryoslice images of the mice were obtained approximately from the same slice imaged *in vivo* and are shown on Fig. 4A.e and Fig. 4A.j respectively. Fluorescence images of LipoICG$_{75}$ (in pseudo-green) were superimposed onto the color image to demonstrate high-congruence of the fluorescence cryoslice images with the non-invasive MSOT *in vivo* findings (Fig. 4A.e, 4A.j). Notably, the SNR is very similar to the one obtained with MSOT (43 dB–44 dB respectively in the 4T1 tumor model), where there is generally absence of fluorescence signal observed in the core of the HT29 tumor, even though some peripheral activity is present in both Fig. 4A.i and 4A.j. Fig. 4A.i and 4A.j show a small discrepancy between fluorescent and MSOT signal localization, predominantly due to photons easily diffusing through the thickness of the sample around the tumor during fluorescence picture acquisition, compared to the strongly absorbing body, artificially increasing tumor signal. This originates Cryoslice imaging of other mouse tissues (liver, kidney, spleen) in the abdominal cavity of tumor bearing animals was performed, and representative images (Fig. 4D.a, D.c for MSOT and 4D.b, D.d for cryosections) confirmed intense signals coming primarily from the liver and partly from the spleen, as shown in more detail in Fig. 2. Again raw signals, not corrected for fluence effects are shown here, to demonstrate the raw capacity of MSOT to resolve signals with depth, in analogy to Fig. 2C.

The MSOT data obtained *in vivo* in the 4T1 tumor model were analyzed to extract LipoICG$_{75}$ signal intensity values in different mouse areas including the tumor, back muscles and an average value from the entire transverse section of the mouse body excluding the tumor. Fig. 4B illustrates the signal intensity in those mouse areas over time. LipoICG$_{75}$ signal in the body shows a high intensity peak a few minutes after the injection, gradually decreasing with time, attributed to the construct circulating in the blood. In contrast, LipoICG$_{75}$ signal from the tumor showed an initial increase with time and reached a plateau 4 h after injection to remain constant during the 24 h, even if the distribution pattern changed from the 4 h to the 24 h time point, as seen in Fig. 4A.c, A.d. Optoacoustic signals collected from the muscle showed a similar pattern to those obtained from the rest of the body although at an apparent faster clearance rate. Fig. 4C shows the increase of tumor-to-muscle and tumor-to-body ratio as a function of time.

To better understand the *in vivo* MSOT observations, histological analysis of the tumor sections was performed. Fig. 5A show reconstitution of complete tumor slices stained with H&E, obtained from two 4T1 tumors harvested at 1 h and 24 h post-injection. Fig. 5B shows in higher resolution H&E, CD31 and fluorescence microscopy images at 805–830 nm (LipoICG$_{75}$ signal) from the areas marked with the three boxes marked on Fig. 5A. Results from both tumors obtained at 1 h and 24 h post-injection are shown. CD31 staining overall confirmed differences in tumor vascularization consistent with the MSOT observations. 1 h after injection, LipoICG$_{75}$ is present in the tumor vasculature, signal that disappears at 24 h (Fig. 5B.d) Conversely LipoICG$_{75}$ signal from the tumor core increases from 1 h to 24 h as seen by contrasting Fig. 5B.c and Fig. 5B.f.

4. Discussion

This study confirmed LipoICG$_{75}$ as a potent agent for clinical optoacoustic contrast and reveals previously unattainable insight of nanoscale vesicle distribution within the tumor microenvironment *in vivo* and non-invasively at ~35 μm resolution. Gold and other metal-based particles emit strong optoacoustic signals but are generally retained over time in different organs, raising toxicity questions [37–39]. Such nanoparticles are not currently considered with a straightforward path to clinical translation. However, they constitute the "gold standard" for optoacoustic imaging thanks to their strong signal generation and overall photo-stability. On the other hand, several agents based on organic dyes and fluorochromes are eliminated rapidly from the body and have received clinical approval. ICG has been granted FDA approval in 1959 and is routinely used in a variety of clinical settings and protocols (ophthalmologic, cardiovascular, etc.) [40]. However, ICG offers a significantly smaller absorption cross-section than metal nanoparticles and has notoriously poor *in vivo* stability (self-aggregation) and rapid blood clearance rate further compromising its imaging utility.

In the present work, we focused on a liposome-based ICG vesicular system considered as an optoacoustic agent. LipoICG$_{75}$ was engineered on molecular self-assembly principles (i.e. no new chemical entities were synthesized) and was made entirely of clinically-approved components. We designed this nanoparticle as a biodegradable and biocompatible nanoscale platform system that could offer high cross-section appropriate for optoacoustic imaging and robust *in vivo* stability and long-term (at least 24 h) blood circulation profile. A first key finding in the study was that, besides its potential for clinical translation, LipoICG$_{75}$ would generate strong optoacoustic signal. Specifically, for an equivalent administered mass, LipoICG$_{75}$ was found to generate stronger optoacoustic signal compared to gold-nanoparticles. This performance was theoretically predicted previously [19] but it is the first time that it is demonstrated experimentally. It represents in itself a major step forward for the modality, as LipoICG surpasses gold for signal generation as well as biocompatibility, presenting a "best of both worlds" approach. The LipoICG$_{75}$ optoacoustic contrast depends on the ability to concentrate optical absorbers within tissue. Free agent at an equivalent concentration yields similar signal generation *ex vivo* (Fig. 3) but when administered at an identical dose to LipoICG$_{75}$ cannot be delivered at the same density *in vivo* (Fig. 2) compared to using liposome packaging.

Previously, liposome systems labeled with ICG have been considered as fluorescent agents for intradermal administration in the footpad region of healthy animals, intended for lymph-node imaging [18,23,24]. The LipoICG vesicles in this study resolve the two main limitations of free ICG for such clinical applications [41,42], namely its low stability in aqueous environments and its strong binding to serum albumin that leads to a dramatic reduction of optical signal after intra-venous injection. The contrast generation performance points to LipoICG$_{75}$ as a potent agent for clinical optoacoustics. LipoICG$_{75}$ can be considered as a perfusion agent for optoacoustic imaging, in particular for visualizing vascular permeability, identify lymphatic systems associated with tumors and as a diagnostic tool prior, during and follow-up after interventions.

Possible clinical indications could combine the intrinsic ability of MSOT to resolve tissue oxygenation/hypoxia, as shown on Fig. 4 with LipoICG$_{75}$ contrast enhancement to impact clinical decision making. Examples include the assessment of hypoxia and perfusion during cardiovascular disease interventions (i.e. bypass surgery) or

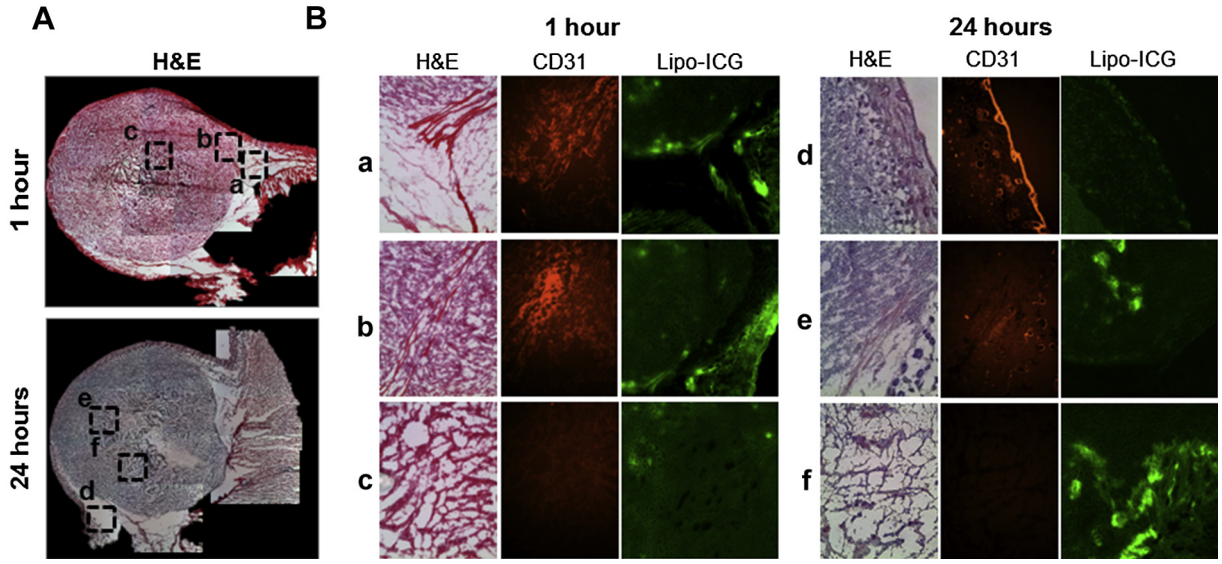

Fig. 5. *Ex-vivo* microscopy study of LipoICG$_{75}$ extravasation in a 4T1 tumor model. (A) Reconstitution of Hematoxylin & Eosin (H&E) staining of complete 4T1 tumor slice 1 h (top) and 24 h (bottom) after injection of liposomal ICG. (B) H&E (color channel), CD31 (red channel) and LipoICG$_{75}$ (green channel) microscopy pictures of various locations of the tumor depicted in (A), a-c for 1 h after LipoICG$_{75}$ injection and d-f for 24 h after LipoICG$_{75}$ injection. (For interpretation of the references to color in this figure legend, the reader is referred to the web version of this article.)

in studying organ function during transplantation surgery. In oncology, knowledge on the perfusion and oxygenation status in solid tumors is of paramount clinical importance. Head- and neck cancer tends to be highly resistant to radio- and chemotherapy due to the presence of hypoxic areas within these tumors. Detailed knowledge on the extent and heterogeneity of hypoxia prior to initiation of standard treatment modalities like radio- and chemotherapy or novel modalities like targeted therapy or photoimmunotherapy may reveal whether a treatment response is to be expected or treatment conditions need to be altered. Moreover, response rates can be repeatedly monitored after installment of therapy.

MSOT compared to fluorescence imaging is advantageous since contrast from the vasculature is shown to be differentiated from any background signal from the tumor mass. Tumor contrast due to enhanced tumor permeability and retention was observed herein within an hour after administration, which implies that clinical use would be possible within a single patient visit. However it is also foreseen that labeled liposomes can be employed to assess the efficacy of payload delivery over longer periods of time, in a theranostics scenario. In this role LipoICG$_{75}$ can be used to optimize therapies and better assess therapeutic efficacy.

The findings in this study also identified MSOT as a potent strategy to understand contrast generation and liposome delivery in general. MSOT could identify the time dynamics of LipoICG$_{75}$ in animals *in vivo*, over long periods of time. The gradual exchange of LipoICG$_{75}$ from blood circulation to tumors was visualized and confirmed against fluorescence cryosections. MSOT was found superior to planar optical imaging systems in visualizing the nanoparticle biodistribution and overall showcased the preferred features of optoacoustics for optical imaging. IVIS imaging of LipoICG and free ICG showed only limited superficial biodistribution information and missed the presence of liver fluorescence at longer time points. Conversely, cross-section MSOT images, revealed accurate congruence with the *ex vivo* validation studies although have not been processed for optical fluence attenuation with depth. The *in vivo* findings were confirmed with *ex vivo* cryoslicing and histology studies and showcased that LipoICG$_{75}$ will offer different distribution and subsequently load delivery patterns depending on the tissue or tumor type.

In this study, we studied the 4T1 cell line that results in a fast growing tumor with a leaky vasculature [35] and contrasted it to the human HT29 colon carcinoma model, which presents slower growth [36] and a restricted microvascular network. These features have been observed using intrinsic tissue contrast (hemoglobin) revealing the anatomy of the vascular system within tumors. The liposome systems ranged between 100 and 150 nm, enabling observations of enhanced permeation and retention [43]. MSOT imaging revealed tumor hypoxia heterogeneity and the LipoICG$_{75}$ extravasation pattern at scalable resolution (Fig. 4). Multispectral imaging could be achieved at video rates, i.e. at least 10 frames per second [44] allowing these observations in a dynamic motion and artifact free fashion.

The ability to interrogate the entire tumor mass with an optical method possibly offers a paradigm shift in oncology and in pharmacology studies. It was shown herein that it is possible to avoid complicated radiolabelling and short-lived imaging or expensive MRI studies of low sensitivity and instead deliver high-resolution longitudinal imaging of optically-labeled delivery vehicles using optoacoustics. In this study we observed a heterogeneous distribution within tumors and a marked variation on the ability to localize within different tumor types. It is well documented that significant physiological and anatomical differences exist among tumor types [45]. MSOT allowed illustration of such differences, opening new paths towards personalization of treatment regimes.

A distinct advantage of MSOT is the use of spectral information to record contrast. The distribution of optical agent does not rely on difference images, i.e. images that are obtained as a subtraction of images before and after agent administration typical in other high-resolution imaging approaches such as X-ray CT, MRI or ultrasound. Rich spectral information is unique to optical methods. When combined with high resolution it offers a unique imaging capabilities, since it significantly enhances the detection sensitivity and specificity. The limitation of the optoacoustic method is the need for laser illumination and the restrictions posed by light penetration (up to ~3 cm from tissue surface). That can also limit its applications to preclinical imaging and localized clinical imaging protocols in endoscopy, surgery, ophthalmology or dermatology.

5. Conclusion

The recent development of optoacoustic imaging equipment for human use [44] offers a realistic platform and need for an effective optoacoustic contrast agent. We foresee LipoICG$_{75}$ playing a major role in the development of clinical optoacoustics paving the road to more sophisticated approaches like targeted moieties. It is also anticipated that this type of contrast agent platform can evolve rapidly to assist in the development of actively (monoclonal antibody or peptide based) targeted moieties against specific cancer types. We believe this work provides a case study on how nanoscale science can corroborate advances in novel imaging modalities to allow the creation of seamless clinical opportunities, with a paradigm shift in clinical decision making.

Competing interests

V.N. is a shareholder of iThera Medical GmbH.

Acknowledgments

The authors would like to thank the Cluster of Excellence “Nanosystem Initiative Munich” and the ERC Advanced Grant (233161) “Next Generation *in vivo* imaging platform for post-genome biology and medicine MSOT” for their financial support. N.L. would like to acknowledge the Andalusian Initiative for Advanced Therapies funded by the Regional Government of Andalusia, Spain. We are grateful to Stratis Tzoumas for his valuable insight in optoacoustic image processing.

Appendix A. Supplementary data

Supplementary data related to this article can be found at http://dx.doi.org/10.1016/j.biomaterials.2014.10.014.

References

[1] Bangham AD, Horne RW. Negative staining of phospholipids and their structural modification by surface-active agents as observed in the electron microscope. J Mol Biol 1964 May;8:660–8.
[2] Al-Jamal WT, Kostarelos K. Liposomes: from a clinically established drug delivery system to a nanoparticle platform for theranostic nanomedicine. Accounts Chem Res 2011 Oct 18;44(10):1094–104.
[3] Sawant RR, Torchilin VP. Liposomes as 'smart' pharmaceutical nanocarriers. Soft Matter 2010;6(17):4026–44.
[4] Schwendener RA, Schott H. Liposome formulations of hydrophobic drugs. Methods Mol Biol 2010;605:129–38. PubMed PMID: 20072877. Epub 2010/01/15. eng.
[5] Gabizon A, Catane R, Uziely B, Kaufman B, Safra T, Cohen R, et al. Prolonged circulation time and enhanced accumulation in malignant exudates of doxorubicin encapsulated in polyethylene-glycol coated liposomes. Cancer Res 1994 Feb 15;54(4):987–92.
[6] Minisini AM, Andreetta C, Fasola G, Puglisi F. Pegylated liposomal doxorubicin in elderly patients with metastatic breast cancer. Expert Rev Anticancer Ther 2008 Mar;8(3):331–42.

[7] Tejada-Berges T, Granai CO, Gordinier M, Gajewski W. Caelyx/Doxil for the treatment of metastatic ovarian and breast cancer. Expert Rev Anticancer Ther 2002 Apr;2(2):143–50.
[8] Iyer AK, Khaled G, Fang J, Maeda H. Exploiting the enhanced permeability and retention effect for tumor targeting. Drug Discov Today 2006;11(17–18):812–8.
[9] Luk BT, Fang RH, Zhang L. Lipid- and polymer-based nanostructures for cancer theranostics. Theranostics 2012;2(12):1117–26. PubMed PMID: 23382770.
[10] Strijkers GJ, Kluza E, Van Tilborg GA, van der Schaft DW, Griffioen AW, Mulder WJ, et al. Paramagnetic and fluorescent liposomes for target-specific imaging and therapy of tumor angiogenesis. Angiogenesis 2010 Jun;13(2):161–73.
[11] Petersen AL, Hansen AE, Gabizon A, Andresen TL. Liposome imaging agents in personalized medicine. Adv Drug Deliv Rev 2012;64(13):1417–35.
[12] Rubesova E, Berger F, Wendland MF, Hong K, Stevens KJ, Gooding CA, et al. Gd-labeled liposomes for monitoring liposome-encapsulated chemotherapy: quantification of regional uptake in tumor and effect on drug delivery. Acad Radiol 2002 Aug;9(Suppl. 2):S525–7.
[13] Viglianti BL, Abraham SA, Michelich CR, Yarmolenko PS, MacFall JR, Bally MB, et al. In vivo monitoring of tissue pharmacokinetics of liposome/drug using MRI: illustration of targeted delivery. Magn Reson Med 2004 Jun;51(6):1153–62.
[14] Badea CT, Athreya KK, Espinosa G, Clark D, Ghafoori AP, Li YF, et al. Computed tomography imaging of primary lung Cancer in mice using a liposomal-iodinated contrast agent. PloS one 2012 Apr 2;7(4).
[15] Zheng J, Allen C, Serra S, Vines D, Charron M, Jaffray DA. Liposome contrast agent for CT-based detection and localization of neoplastic and inflammatory lesions in rabbits: validation with FDG-PET and histology. Contrast Media Mol Imaging 2010 May-Jun;5(3):147–54.
[16] Li S, Goins B, Zhang L, Bao A. Novel multifunctional theranostic liposome drug delivery system: construction, characterization, and multimodality MR, near-infrared fluorescent, and nuclear imaging. Bioconjugate Chem 2012 May 22;23(6):1322–32.
[17] Portnoy E, Lecht S, Lazarovici P, Danino D, Magdassi S. Cetuximab-labeled liposomes containing near-infrared probe for in vivo imaging. Nanomedicine : nanotechnology, biology. Medicine 2011 Aug;7(4):480–8.
[18] Proulx ST, Luciani P, Derzsi S, Rinderknecht M, Mumprecht V, Leroux JC, et al. Quantitative imaging of lymphatic function with liposomal indocyanine green. Cancer Res 2010 Sep 15;70(18):7053–62.
[19] Ntziachristos V, Razansky D. Molecular imaging by means of multispectral optoacoustic tomography (MSOT). Chem Rev 2010;110(5):2783–94.
[20] Zha Z, Deng Z, Li Y, Li C, Wang J, Wang S, et al. Biocompatible polypyrrole nanoparticles as a novel organic photoacoustic contrast agent for deep tissue imaging. Nanoscale 2013 May 21;5(10):4462–7.
[21] Lovell JF, Jin CS, Huynh E, Jin HL, Kim C, Rubinstein JL, et al. Porphysome nanovesicles generated by porphyrin bilayers for use as multimodal biophotonic contrast agents. Nat Mater 2011 Apr;10(4):324–32.
[22] Ng KK, Shakiba M, Huynh E, Weersink RA, Roxin A, Wilson BC, et al. Stimuli-responsive photoacoustic nanoswitch for in vivo sensing applications. ACS nano 2014 Jul 28;8(8):8363–73.
[23] Zhuang Y, Ma Y, Wang C, Hai L, Yan C, Zhang Y, et al. PEGylated cationic liposomes robustly augment vaccine-induced immune responses: role of lymphatic trafficking and biodistribution. J Control Release 2012 Apr 10;159(1):135–42.
[24] Jeong HS, Lee CM, Cheong SJ, Kim EM, Hwang H, Na KS, et al. The effect of mannosylation of liposome-encapsulated indocyanine green on imaging of sentinel lymph node. J Liposome Res 2013 Dec;23(4):291–7.
[25] Buehler A, Herzog E, Razansky D, Ntziachristos V. Video rate optoacoustic tomography of mouse kidney perfusion. Opt Lett 2010 Jul 15;35(14):2475–7.
[26] Buehler A, Rosenthal A, Jetzfellner T, Dima A, Razansky D, Ntziachristos V. Model-based optoacoustic inversions with incomplete projection data. Med Phys 2011 Mar;38(3):1694–704.
[27] Rosenthal A, Razansky D, Ntziachristos V. Fast semi-analytical model-based acoustic inversion for quantitative optoacoustic tomography. IEEE Trans Med Imaging 2010 Jun;29(6):1275–85.
[28] Razansky D, Distel M, Vinegoni C, Ma R, Perrimon N, Koster RW, et al. Multispectral opto-acoustic tomography of deep-seated fluorescent proteins in vivo. Nat Photonics 2009 Jul;3(7):412–7.
[29] Ntziachristos V, Ripoll J, Wang LV, Weissleder R. Looking and listening to light: the evolution of whole-body photonic imaging. Nat Biotechnol 2005 Mar;23(3):313–20.
[30] Hong RL, Huang CJ, Tseng YL, Pang VF, Chen ST, Liu JJ, et al. Direct comparison of liposomal doxorubicin with or without polyethylene glycol coating in C-26 tumor-bearing mice: is surface coating with polyethylene glycol beneficial? Clinical cancer research. official J Am Assoc Cancer Res 1999 Nov;5(11):3645–52.
[31] Al-Jamal WT, Al-Ahmady ZS, Kostarelos K. Pharmacokinetics & tissue distribution of temperature-sensitive liposomal doxorubicin in tumor-bearing mice triggered with mild hyperthermia. Biomaterials 2012 Jun;33(18):4608–17.
[32] Herzog E, Taruttis A, Beziere N, Lutich AA, Razansky D, Ntziachristos V. Optical imaging of cancer heterogeneity with multispectral optoacoustic tomography. Radiology 2012 May;263(2):461–8.
[33] Bao C, Beziere N, del Pino P, Pelaz B, Estrada G, Tian F, et al. Gold nanoprisms as optoacoustic signal nanoamplifiers for in vivo bioimaging of gastrointestinal cancers. Small 2013 Jan 14;9(1):68–74.
[34] Lozano N, Al-Jamal WT, Taruttis A, Beziere N, Burton NC, Van den Bossche J, et al. Liposome-gold nanorod hybrids for high-resolution visualization deep in tissues. J Am Chem Soc 2012 Aug 15;134(32):13256–8.
[35] Demers M, Ho-Tin-Noe B, Schatzberg D, Yang JJ, Wagner DD. Increased efficacy of breast cancer chemotherapy in thrombocytopenic mice. Cancer Res 2011 Mar 1;71(5):1540–9.
[36] Fogh J, Fogh JM, Orfeo T. One hundred and twenty-seven cultured human tumor cell lines producing tumors in nude mice. J Natl Cancer Inst 1977 Jul;59(1):221–6.
[37] Kostarelos K. The long and short of carbon nanotube toxicity. Nat Biotechnol 2008 Jul;26(7):774–6.
[38] Simeonova PP. Update on carbon nanotube toxicity. Nanomedicine (Lond) 2009 Jun;4(4):373–5.
[39] Zhang XD, Wu D, Shen X, Liu PX, Yang N, Zhao B, et al. Size-dependent in vivo toxicity of PEG-coated gold nanoparticles. Int J nanomedicine 2011;6:2071–81.
[40] Alander JT, Kaartinen I, Laakso A, Patila T, Spillmann T, Tuchin VV, et al. A review of indocyanine green fluorescent imaging in surgery. Int J Biomed Imaging 2012;2012:940585.
[41] Gathje J, Steuer RR, Nicholes KR. Stability studies on indocyanine green dye. J Appl Physiol 1970 Aug;29(2):181–5.
[42] Desmettre T, Devoisselle JM, Mordon S. Fluorescence properties and metabolic features of indocyanine green (ICG) as related to angiography. Surv Ophthalmol 2000 Jul-Aug;45(1):15–27.
[43] Maeda H, Wu J, Sawa T, Matsumura Y, Hori K. Tumor vascular permeability and the EPR effect in macromolecular therapeutics: a review. J Control Release 2000;65(1–2):271–84.
[44] Buehler A, Kacprowicz M, Taruttis A, Ntziachristos V. Real-time handheld multispectral optoacoustic imaging. Opt Lett 2013 May 1;38(9):1404–6.
[45] Hanahan D, Weinberg RA. Hallmarks of cancer: the next generation. Cell. 2011 Mar 4;144(5):646–74.